Author(s): Heikkola, Erkki; Mönkölä, Sanna; Pennanen, Anssi; Rossi, Tuomo

Title: Controllability method for acoustic scattering with spectral elements

Year: 2007

Version:

Please cite the original version:

Heikkola, E., Mönkölä, S., Pennanen, A., & Rossi, T. (2007). Controllability method for acoustic scattering with spectral elements. Journal of Computational and Applied Mathematics, 204(2), 344-355. https://doi.org/10.1016/j.cam.2006.02.046

Controllability method for acoustic scattering with spectral elements

Erkki Heikkola [a] Sanna Mönkölä [b,*] Anssi Pennanen [b]
Tuomo Rossi [b]

[a] *Numerola Oy, P.O. Box 126, FI-40101 Jyväskylä, Finland*

[b] *Department of Mathematical Information Technology, P.O. Box 35 (Agora), FI-40014 University of Jyväskylä, Finland*

Abstract

We formulate the Helmholtz equation as an exact controllability problem for the time-dependent wave equation. The problem is then discretized in time domain with central finite difference scheme and in space domain with spectral elements. This approach leads to high accuracy in spatial discretization. Moreover, the spectral element method results in diagonal mass matrices, which makes the time integration of the wave equation highly efficient. After discretization, the exact controllability problem is reformulated as a least squares problem, which is solved by the conjugate gradient method. We illustrate the method with some numerical experiments, which demonstrate the significant improvements in efficiency due to the higher order spectral elements. For a given accuracy, the controllability technique with spectral element method requires fewer computational operations than with conventional finite element method. In addition, by using higher order polynomial basis the influence of the pollution effect is reduced.

Key words: Exact controllability, Helmholtz equation, Spectral element method, Mass lumping
PACS: 43.20

1 Introduction

The Helmholtz equation is a fundamental equation for time-harmonic wave propagation. It occurs in a number of physical applications such as underwater

* Corresponding author.
Email address: sanna.monkola@it.jyu.fi (Sanna Mönkölä).

Article published in Journal of Computational and Applied Mathematics 204 (2) (2007) 344–355

acoustics, medicine, and geophysics. It can also be used to model the scattering of time-harmonic acoustic waves by an obstacle.

We consider a controllability method for the numerical solution of the two-dimensional Helmholtz equation with an absorbing boundary condition describing the scattering of a time-harmonic incident wave by a sound-soft obstacle:

$$-\omega^2 U - \nabla^2 U = F, \qquad \text{in } \Omega, \tag{1}$$

$$U = 0, \qquad \text{on } \Gamma_0, \tag{2}$$

$$-i\omega U + \frac{\partial U}{\partial \mathbf{n}} = Y_{\text{ext}}, \qquad \text{on } \Gamma_{\text{ext}}. \tag{3}$$

Function $U(\mathbf{x})$ denotes the total acoustic pressure consisting of the scattered wave $U_{\text{scat}}(\mathbf{x})$ and the incident wave $U_{\text{inc}}(\mathbf{x}) = \exp(i\vec{\omega} \cdot \mathbf{x})$, where i is the imaginary unit and the vector $\vec{\omega}$ gives the propagation direction. The angular frequency is denoted by $\omega = \|\vec{\omega}\|_2$, and the corresponding wavelength is given by $\lambda = \frac{2\pi}{\omega}$. In a problem formulated this way, the wavenumber is equal to the angular frequency. Functions Y_{ext} and F in the equations above depend on the incident wave, and are of the form

$$F = -\omega^2 U_{\text{inc}}(\mathbf{x}) - \nabla^2 U_{\text{inc}}(\mathbf{x}), \tag{4}$$

$$Y_{\text{ext}} = -i\omega U_{\text{inc}}(\mathbf{x}) + \frac{\partial U_{\text{inc}}(\mathbf{x})}{\partial \mathbf{n}}, \tag{5}$$

where $\mathbf{n}$ is the outward normal vector to domain Ω. In scattering problems with constant wave number the right-hand side function F is zero, but it becomes nonzero with nonconstant ω. Here we keep ω constant but the controllability method is not restricted in this respect.

The domain Ω is bounded by the surface of the obstacle Γ_0 and an absorbing boundary Γ_{ext} (see Fig. 1). On the absorbing boundary Γ_{ext}, we impose the conventional first order boundary condition [1]. This is the simplest alternative and not accurate in approximating the Sommerfeld radiation condition. However, it is sufficient for the presentation of the controllability method of this article. We shall consider more sophisticated boundary conditions and absorbing layers in future.

Many solution techniques have been proposed for the Helmholtz equation (1)-(3). For example, various fictitious domain and domain decomposition methods have been applied to the corresponding finite element problems. A common quality of these methods is that they lead to large-scale indefinite linear systems, which are solved iteratively. It is difficult to develop efficient preconditioners for the iterative solution, especially if the material coefficients are varying. Preconditioners for solving the Helmholtz equation are considered in [2] and [3], and multigrid based preconditioning introduced in [3] has given

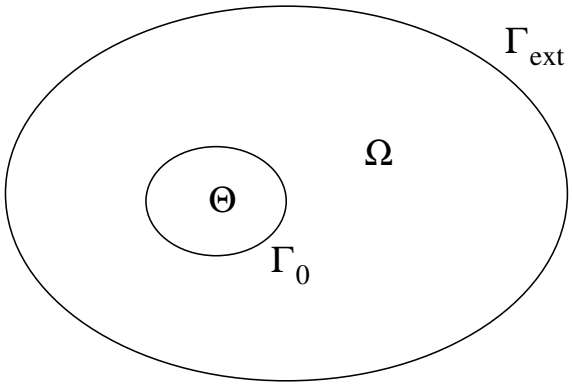

Figure 1. Obstacle Θ, domain Ω, and the two parts of the boundary $\partial\Omega = \Gamma_0 \cup \Gamma_{\text{ext}}$ of the domain Ω.

promising results.

Another difficulty in the finite element solution of the Helmholtz equation is the pollution effect, which deteriorates accuracy when wave number increases even if discretization resolution is kept fixed (see, e.g., [4]). Many techniques have been developed to reduce the pollution effect and during recent years various methods using plane waves as basis functions have turned out to be succesful (see, e.g., [5], [6]). In this work, we adhere to a polynomial basis, but increase the order of the basis functions to reduce the pollution effect.

We use the idea of Bristeau, Glowinski, and Périaux presented in [7] to formulate the Helmholtz problem as an exact controllability problem for the time-dependent wave equation. Exact controllability approach is inspired by the Hilbert Uniqueness Method (HUM) introduced by Lions [8] as a systematic method to address controllability problems for partial differential equations. This controllability technique was used also in [9], where it was combined with a fictitious domain method, and Lagrange multipliers were used to handle the Dirichlet condition.

As in [10], we discretize the wave equation in space domain with spectral elements, which combines the geometric flexibility of finite elements with the high accuracy of spectral methods. The basis functions are higher order Lagrange interpolation polynomials, and the nodes of these functions are placed at Gauss-Lobatto (GL) collocation points. The integrals in the weak form of the equation are evaluated with the corresponding Gauss-Lobatto quadrature formulas. As a consequence of the choice, the mass matrix is diagonal.

We use the central finite difference scheme for time discretization. This scheme is second order accurate and with a diagonal mass matrix also fully explicit, which are both essential properties for computational efficiency. Only matrix-vector products are needed in time-dependent simulation, but the scheme needs to satisfy the CFL condition, which limits the length of the time step

(see [10] for details).

After discretization, exact controllability problem is reformulated as a least squares problem, which is solved with the preconditioned conjugate gradient (CG) algorithm. Computation of the gradient of the function to be minimized is an essential stage of the method. This is performed by the adjoint equation technique. In [7], the gradient was derived on the continuous level, and the same formula was used also on the discrete level. We discretize first the wave equation and the function to be minimized. Then, we compute the gradient directly for the discretized problem.

The rest of the paper is organized as follows: The formulation of the exact controllability problem is considered in Section 2. The discretization of the exact controllability problem is described in Section 3. In Section 4, we present the least-squares problem and consider its conjugate gradient solution. Finally, in Section 5, we study the performance of the method with numerical experiments.

2 Exact controllability formulation

Instead of solving directly the time-harmonic equation, we return to the corresponding time-dependent equation and look for time-periodic solution. Direct time-integration of the wave equation can be used to reach the time-periodic case, but convergence is usually too slow to be useful in practice. As the results in [7] indicate, the convergence can be vastly improved by control techniques.

Solution of the time-harmonic equation (1)-(3) is equivalent to finding a periodic solution for the corresponding time-dependent wave equation. The period T corresponding to the angular frequency ω is given by $\frac{2\pi}{\omega}$, and the T- periodic solution can be achieved by controlling the initial conditions such that the solution and its first time derivative at time T coincide with the initial conditions.

We introduce the Hilbert space Z for the initial conditions $\mathbf{e} = (e_0, e_1) \in Z$ by

$$Z = V \times L^2(\Omega), \tag{6}$$

where

$$V = \{v \in H^1(\Omega) \text{ such that } v = 0 \text{ on } \Gamma_0\}. \tag{7}$$

Then, we have the following exact controllability problem: Find initial conditions $\mathbf{e} \in Z$ such that equations

$$\frac{\partial^2 u}{\partial t^2} - \nabla^2 u = f, \qquad \text{in } Q = \Omega \times [0,T], \tag{8}$$

$$u = 0, \qquad \text{on } \gamma_0 = \Gamma_0 \times [0,T], \tag{9}$$

$$\frac{\partial u}{\partial t} + \frac{\partial u}{\partial \mathbf{n}} = y_{\text{ext}}, \qquad \text{on } \gamma_{\text{ext}} = \Gamma_{\text{ext}} \times [0,T], \tag{10}$$

$$u(\mathbf{x},0) = e_0, \quad \frac{\partial u}{\partial t}(\mathbf{x},0) = e_1 \qquad \text{in } \Omega, \tag{11}$$

$$u(\mathbf{x},T) = e_0, \quad \frac{\partial u}{\partial t}(\mathbf{x},T) = e_1 \qquad \text{in } \Omega, \tag{12}$$

hold with

$$f(\mathbf{x},t) = -\omega^2 u_{\text{inc}}(\mathbf{x},t) - \nabla^2 u_{\text{inc}}, \tag{13}$$

$$y_{\text{ext}}(\mathbf{x},t) = \frac{\partial u_{\text{inc}}(\mathbf{x},t)}{\partial \mathbf{n}} - \text{Re}(i\omega U_{\text{inc}} \exp(-i\omega t)), \tag{14}$$

where $u_{\text{inc}}(\mathbf{x},t) = \text{Re}(U_{\text{inc}}(\mathbf{x}) \exp(-i\omega t))$. When the exact controllability problem is solved, the complex-valued solution U of (1)-(3), is obtained by $U = e_0 + \frac{i}{\omega} e_1$.

The spectral element discretization of the problem is based on the weak formulation of the classical wave equation (8)-(10): Find u satisfying $u(t) \in V$ for any $t \in [0,T]$ and

$$\begin{aligned} \int_\Omega \frac{\partial^2 u}{\partial t^2} v \, dx + \int_\Omega \nabla u \cdot \nabla v \, dx + \int_{\Gamma_{\text{ext}}} \frac{\partial u}{\partial t} v \, ds \\ = \int_\Omega f v \, dx + \int_{\Gamma_{\text{ext}}} y_{\text{ext}} v \, ds \end{aligned} \tag{15}$$

for any $v \in V$ and $t \in [0,T]$.

3 Discretization

For the spatial discretization of the wave equation (8)-(11), we use spectral element method, which combines the geometric flexibility of classical finite elements with the high accuracy of spectral methods. The computational domain is divided into quadrilateral elements, and in each element a local higher order polynomial basis is introduced. The degrees of freedom corresponding to the basis functions are located at the Gauss-Lobatto integration points of the elements. This method is especially useful for the solution of time-dependent wave equations, because it leads to a diagonal mass matrix also with a higher order basis [10] (see also [11]). This fact is very beneficial for the time-dependent simulation with explicit schemes. After spatial discretization we have the semi-discrete equation

$$\mathcal{M}\frac{\partial^2 \mathbf{u}}{\partial t^2} + \mathcal{S}\frac{\partial \mathbf{u}}{\partial t} + \mathcal{K}\mathbf{u} = \mathcal{F}, \tag{16}$$

where vector $\mathbf{u}(t)$ contains the nodal values of the function $u(\mathbf{x}, t)$ at time t, and satisfies the initial condition (11) at time $t = 0$. Because both the mass matrix $\mathcal{M}$ and the matrix $\mathcal{S}$ are diagonal, explicit time stepping with central finite differences requires only matrix-vector multiplications. Stiffness matrix is denoted by $\mathcal{K}$, and $\mathcal{F}$ is the vector due to the functions f and y_{ext}.

The time discretization of the semi-discrete equation is performed with the standard central finite differences. This method is second order accurate with respect to the timestep Δt and leads to an explicit time-stepping scheme. Both properties are essential for computational efficiency.

The time interval $[0, T]$ is divided into N timesteps, each of size $\Delta t = T/N$. After replacing the time derivatives in the semidiscretized form (16) by the appropriate approximations and taking into account the initial condition (11) we obtain the fully discrete state equation, which can be represented in the matrix form

$$\begin{pmatrix} \mathcal{I} & & & & & \\ \mathcal{C}_0 & \mathcal{M} & & & & \\ \mathcal{B} & \mathcal{C} & \mathcal{D} & & & \\ & \ddots & \ddots & \ddots & & \\ & & \mathcal{B} & \mathcal{C} & \mathcal{D} & \\ & & & \mathcal{B} & \mathcal{C} & \mathcal{D} \end{pmatrix} \begin{pmatrix} u^0 \\ u^1 \\ \vdots \\ \vdots \\ u^N \\ u^{N+1} \end{pmatrix} - \begin{pmatrix} \mathcal{I} & 0 \\ 0 & \Delta t\,\mathcal{B} \\ 0 & 0 \\ \vdots & \vdots \\ \vdots & \vdots \\ 0 & 0 \end{pmatrix} \begin{pmatrix} e_0 \\ e_1 \end{pmatrix} - \Delta t^2 \begin{pmatrix} 0 \\ \frac{1}{2}\mathcal{F}^0 \\ \mathcal{F}^1 \\ \vdots \\ \vdots \\ \mathcal{F}^N \end{pmatrix} = 0, \tag{17}$$

where u^i and $\mathcal{F}^i$ are the vectors u and $\mathcal{F}$ at time $i\Delta t$, and e_0 and e_1 are the initial conditions. The matrix blocks $\mathcal{C}_0$, $\mathcal{B}$, $\mathcal{C}$ and $\mathcal{D}$ are given by the formulas

$$\mathcal{C}_0 = \frac{\Delta t^2}{2}\mathcal{K} - \mathcal{M}, \tag{18}$$

$$\mathcal{D} = \mathcal{M} + \frac{\Delta t}{2}\mathcal{S}, \tag{19}$$

$$\mathcal{C} = \Delta t^2\mathcal{K} - 2\mathcal{M}, \tag{20}$$

$$\mathcal{B} = \mathcal{M} - \frac{\Delta t}{2}\mathcal{S}, \tag{21}$$

while $\mathcal{I}$ is the identity matrix. In the next section, when describing the control algorithm, we use for the state equation the short form

$$s(\mathbf{e}, \mathbf{u}(\mathbf{e})) = 0, \tag{22}$$

where $\mathbf{e} = (e_0, e_1)^T$ contains the initial values and $\mathbf{u}$ the vectors u^i. We denote the state equation by $s_0(\mathbf{e}, \mathbf{u}(\mathbf{e})) = 0$ in the special case with $\mathcal{F}^i = 0$ for all i.

4 Control problem

The exact controllability problem for computing T-periodic solution for the wave equation involves finding such initial conditions e_0 and e_1 that the solution u and its time derivative $\frac{\partial u}{\partial t}$ at time T would coincide with the initial conditions. For the numerical solution, the exact controllability problem is replaced by a least-squares optimization problem with the functional J, which is, on the discrete level, of the form:

$$J(e_0, e_1, \mathbf{u}) = \frac{1}{2}\left(u^N - e_0\right)^T \mathcal{K}\left(u^N - e_0\right) + \frac{1}{2}\left(\frac{\partial u^N}{\partial t} - e_1\right)^T \mathcal{M}\left(\frac{\partial u^N}{\partial t} - e_1\right), \tag{23}$$

where $\frac{\partial u^N}{\partial t} = \frac{u^{N+1} - u^{N-1}}{2\Delta t}$ and u^i, $i = N-1, N, N+1$, are given by equation (17).

The purpose is to minimize functional J, which depends on the initial conditions both directly and indirectly through the solution of the wave equation (8)-(11).

Since vector $\mathbf{u}$ depends linearly on the initial conditions e_0 and e_1, J is a quadratic function, and (23) can be minimized by solving the linear system

$\nabla J(e_0, e_1) = 0$. This is performed by an optimization algorithm which requires the gradient of the functional J with respect to the control variables e_0 and e_1.

Our algorithm differs from the one in [7] with respect to the spatial discretization and the gradient computation. In [7], the gradient was derived on the continuous level, and the same formula was used also on the discrete level. This approach does not lead exactly to the gradient of the function to be minimized. That is why we proceed in different order and discretize the problem before deriving the gradient formulas. However, our experiments in [12] indicate that the two ways to compute the gradient lead to practically the same convergence for the CG method.

By the adjoint equation technique we see that

$$\frac{dJ(\mathbf{e}, \mathbf{u}(\mathbf{e}))}{de_k} = \frac{\partial J(\mathbf{e}, \mathbf{u})}{\partial e_k} - \mathbf{p}^T \frac{\partial s(\mathbf{e}, \mathbf{u})}{\partial e_k}, \quad k = 0, 1, \tag{24}$$

where $\mathbf{p}$ is the solution of the adjoint equation

$$\left(\frac{\partial s(\mathbf{e}, \mathbf{u})}{\partial \mathbf{u}}\right)^T \mathbf{p} = \left(\frac{\partial J(\mathbf{e}, \mathbf{u})}{\partial \mathbf{u}}\right)^T. \tag{25}$$

In the matrix form corresponding to (17) this equation is given by

$$\begin{pmatrix} \mathcal{I} & \mathcal{C}_0 & \mathcal{B} & & & \\ & \mathcal{M} & \mathcal{C} & \mathcal{B} & & \\ & & \mathcal{D} & \ddots & \ddots & \\ & & & \ddots & \ddots & \mathcal{B} \\ & & & & \mathcal{D} & \mathcal{C} \\ & & & & & \mathcal{D} \end{pmatrix} \begin{pmatrix} p^0 \\ p^1 \\ \vdots \\ \vdots \\ p^N \\ p^{N+1} \end{pmatrix} = \begin{pmatrix} 0 \\ \vdots \\ 0 \\ \frac{\partial J}{\partial u^{N-1}} \\ \frac{\partial J}{\partial u^N} \\ \frac{\partial J}{\partial u^{N+1}} \end{pmatrix}, \tag{26}$$

where

$$\frac{\partial J}{\partial u^{N-1}} = \frac{1}{2\Delta t}\mathcal{M}(e_1 - \frac{\partial u^N}{\partial t}), \tag{27}$$

$$\frac{\partial J}{\partial u^{N+1}} = \frac{1}{2\Delta t}\mathcal{M}(\frac{\partial u^N}{\partial t} - e_1), \tag{28}$$

$$\frac{\partial J}{\partial u^N} = \mathcal{K}(u^N - e_0). \tag{29}$$

The gradient components are then the following:

$$\frac{dJ(\mathbf{e}, \mathbf{u}(\mathbf{e}))}{de_0} = \mathcal{K}(e_0 - u^N) + p^0, \tag{30}$$

$$\frac{dJ(\mathbf{e}, \mathbf{u}(\mathbf{e}))}{de_1} = \mathcal{M}\Big(e_1 - \frac{\partial u^N}{\partial t}\Big) + \Delta t \mathcal{B} p^1. \tag{31}$$

We solve the least squares problem with a preconditioned conjugate gradient (CG) method. The transition procedure to compute the initial approximation of e_0 and e_1 for the CG algorithm is the same as in [7] as well as the block-diagonal preconditioner

$$\mathcal{L} = \begin{pmatrix} \mathcal{K} & 0 \\ 0 & \mathcal{M} \end{pmatrix}. \tag{32}$$

Each CG iteration step requires computation of the gradient ∇J, which involves the solution of the state equation (17) and its adjoint equation (26). Also solution of one linear system with matrix $\mathcal{L}$ and some matrix-vector operations are needed.

Solution of a linear system with the preconditioner requires the solution of systems with the stiffness matrix $\mathcal{K}$ and the diagonal mass matrix $\mathcal{M}$. Efficient solution of linear systems with the matrix $\mathcal{K}$ is critical for the overall efficiency of the control method. At this stage, we use a modification of Kickinger's [13] algebraic multigrid (AMG) introduced in [14]. The use of AMG methods for spectral elements has recently been studied in [15].

Values of the control variables $\mathbf{e}$ at the ith iteration are denoted by e_0^i and e_1^i. Solution of the adjoint state equation is $\mathbf{p} = (p^0, \frac{\partial p^0}{\partial t})$, and the gradient variable is $\mathbf{g} = (g_0, g_1)$. By $s_0(\mathbf{e}, \mathbf{u}(\mathbf{e})) = 0$ we denote the state equation (17), where $\mathcal{F}^i = 0$ for all i. Then, the CG algorithm for solving the least-squares problem is the following:

Algorithm 1 *Preconditioned CG algorithm*

Compute the initial values e_0^0 *and* e_1^0.
Solve the state equation $s(\mathbf{e}^0, \mathbf{u}(\mathbf{e}^0)) = 0$.
Solve the adjoint state equation $\left(\frac{\partial s(\mathbf{e}^0, \mathbf{u}(\mathbf{e}^0))}{\partial \mathbf{u}(\mathbf{e}^0)}\right)^T \mathbf{p} = \left(\frac{\partial J(\mathbf{e}^0, \mathbf{u}(\mathbf{e}^0))}{\partial \mathbf{u}(\mathbf{e}^0)}\right)^T$.
Compute the gradient vectors g_0 *and* g_1 *by the formulas* (30) *and* (31).
Solve linear system with the preconditioner $\mathcal{L}\mathbf{w} = -\mathbf{g}$.
Set $c_0 = -(\mathbf{w}, \mathbf{g})$, $c = c_0$ *and* $i = 1$.
Repeat until norm $< \varepsilon$
Solve the state equation $s_0(\mathbf{w}, \mathbf{u}(\mathbf{w})) = 0$.
Solve the adjoint state equation $\left(\frac{\partial s(\mathbf{w}, \mathbf{u}(\mathbf{w}))}{\partial \mathbf{u}(\mathbf{w})}\right)^T \mathbf{p} = \left(\frac{\partial J(\mathbf{w}, \mathbf{u}(\mathbf{w}))}{\partial \mathbf{u}(\mathbf{w})}\right)^T$.
Compute the gradient updates v_0 *and* v_1 *by the formulas* (30) *and* (31).
Compute $\rho = \frac{c}{(\mathbf{w}, \mathbf{v})}$.
$\mathbf{e}^i = \mathbf{e}^{i-1} + \rho \mathbf{w}$.
$\mathbf{g} = \mathbf{g} + \rho \mathbf{v}$.
Solve linear system with the preconditioner $\mathcal{L}\mathbf{v} = -\mathbf{g}$.
$\gamma = \frac{1}{c}$, $c = -(\mathbf{v}, \mathbf{g})$, $\gamma = c\gamma$.
$\mathbf{w} = \mathbf{v} + \gamma \mathbf{w}$, $i = i + 1$,

where *norm* is either absolute or relative euclidean norm of the variable c, which is the gradient of the functional J.

5 Numerical examples

In order to validate the method, we consider the solution of various test problems. The main purpose of the tests is to study the accuracy of the spectral element discretization and its influence on the efficiency of the method. We also demonstrate the application of the method to some sample scattering problems. Mesh generator provided by Numerola Ltd. is used to divide the computational domain into square elements, each having a side length h. Numerical experiments have been performed on an HP 9000/785/J5600 workstation at 552MHz PA-RISC 8600 CPU.

The time discretization scheme used here is only second order accurate. In connection with higher order elements, the temporal error is larger than the spatial error, unless time steps are very small. Therefore, the number of timesteps is chosen such that stability and accuracy demands are ensured also for higher orders.

5.1 Accuracy of the spatial discretization

There are five factors which affect the accuracy of the final solution to the controllability problem.

(1) spatial discretization, which is performed by the spectral element method,
(2) time discretization, which is performed by central finite differences,
(3) approximation of the geometrical boundaries, which is piecewise linear,
(4) stopping criteria of the CG method, which sets a lower bound for the error,
(5) approximation of the radiation condition.

In the first tests, the aim is to study the accuracy of the spatial approximation, and we try to eliminate or isolate the other factors from the solution. Firstly, we use only such geometrical shapes, which can be approximated exactly by the spectral element mesh. Secondly, we modify the right-hand side function of the problem such that we know the analytic solution. This modification eliminates factor 5 from the error. Thirdly, we use a high number of time steps to reduce the time discretization error. Stopping criteria of the CG method can not be eliminated, but manifests itself as a lower bound for the error and can thus be easily controlled.

The boundary Γ_{ext} coincides with a rectangle with the lower left corner at the point $(0.0, 0.0)$ and the upper right corner at the point $(4.0, 4.0)$. In the center of this rectangle, we have a square obstacle Θ with side length 2. We modify the functions in the scattering problem such that the analytic solution of the problem is known to be the plane wave u_{inc}. For this purpose, we introduce an auxiliary function $\hat{y} \in H^1(\Omega)$ which satisfies the conditions $u_{\text{inc}}(\mathbf{x}, t) = \cos(\omega t - \vec{\omega} \cdot \mathbf{x})$, $\vec{\omega} = \omega\Big(-\frac{1}{\sqrt{2}}, \frac{1}{\sqrt{2}}\Big)$, $\hat{y}|_{\Gamma_0} = u_{\text{inc}}$, $\hat{y}|_{\Gamma_{\text{ext}}} = \frac{\partial \hat{y}}{\partial \mathbf{n}}|_{\Gamma_{\text{ext}}} = 0$, and $y_{\text{ext}} = \frac{\partial u_{\text{inc}}}{\partial t} + \frac{\partial u_{\text{inc}}}{\partial \mathbf{n}}$.

Then, the function $\hat{u}$ defined by $\hat{u} = u - \hat{y}$ satisfies equation (8) with the nonzero right-hand side $f = -\frac{\partial^2 \hat{y}}{\partial t^2} + \nabla^2 \hat{y}$ as well as equations (9) and (10). After solving $\hat{u}$, solution to the actual test problem is given by $u = \hat{u} + \hat{y}$. In these experiments, we have chosen to use 300 timesteps per one time period $[0, T]$, and the stopping criterion works with $norm = \sqrt{\frac{c}{c_0}}$ and $\varepsilon = 10^{-5}$.

In the first experiment, we construct a mesh with $h = 1/4$ in the computational domain. This mesh is used to solve the test problem with wavenumbers $\omega = \pi$ and $\omega = 2\pi$. The mesh resolution is given by $\lambda/h = 2\pi/\omega h$. Fig. 2 shows the error when the order of the spectral basis is increased. As the order increases, the error decreases until the error of the time discretization or the stopping criterion is achieved.

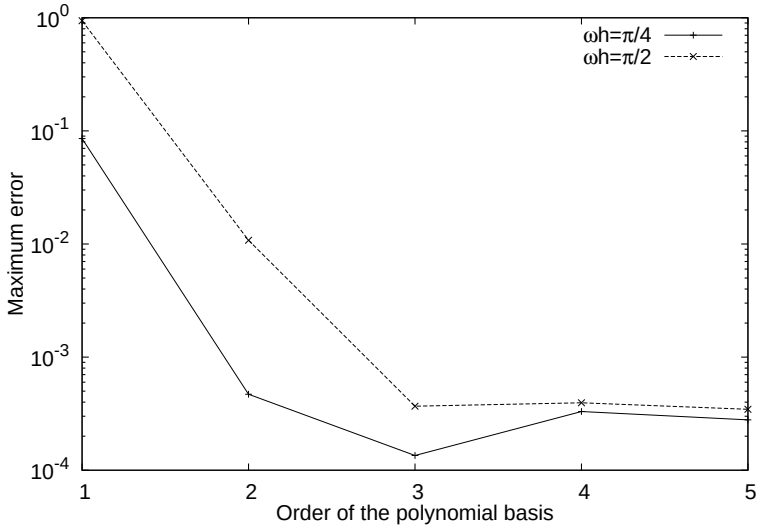

Figure 2. Maximum error with respect to the order of the polynomial basis for two different values of the mesh resolution such that $h = 1/4$.

The number of non-zero entries in the stiffness matrix is essential for computational efficiency, since the time stepping scheme involves mainly matrix-vector multiplications. We extend the first experiment by studying the error in terms of the number of nonzero matrix entries. The results of Fig. 2 are repeated in Fig. 3 as r-refinement. The error curves of the h-refinement are obtained by keeping the order fixed ($r = 1$) and doubling the resolution of the mesh consecutively. Based on the results, it seems clear that it is better to increase the order than the resolution to improve efficiency.

This conclusion is further supported by Fig. 4, which shows the CPU times for these experiments. Naturally the CPU time increases as the resolution or the order is increased but it seems to depend linearly on the number of nonzero entries in the stiffness matrix. The conclusion, that total CPU time for the SEM is much less than the total CPU time for the FEM for same accuracy, follows from these findings. To show the benefit of preconditioning, computations corresponding to h- and r-refinement with $\omega = 2\pi$ are repeated without preconditioning (see Fig. 4). The preconditioned minimization seems to be at least an order of magnitude faster, and CPU time required by the AMG preconditioner is less than 3% of the CPU time for the whole algorithm. Thus, significant savings result from the AMG preconditioner.

We performed another set of experiments by varying the resolution of the mesh with the order of the basis. More specifically we used lower resolution with higher orders according to the equation $\lambda/h = 2^{7-r}$. Fig. 5 shows the error with respect to increasing wavenumber for orders 1-5. The effect of the

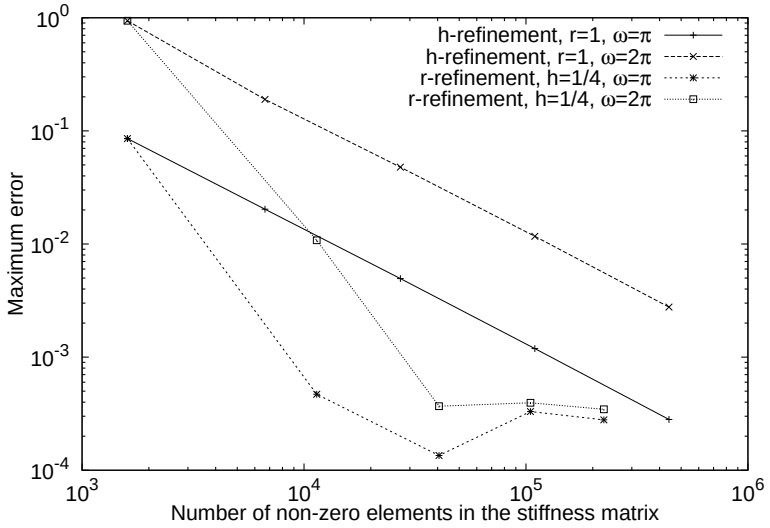

Figure 3. Maximum errors of h- and r-refinements with respect to the number of non-zero elements in the stiffness matrix.

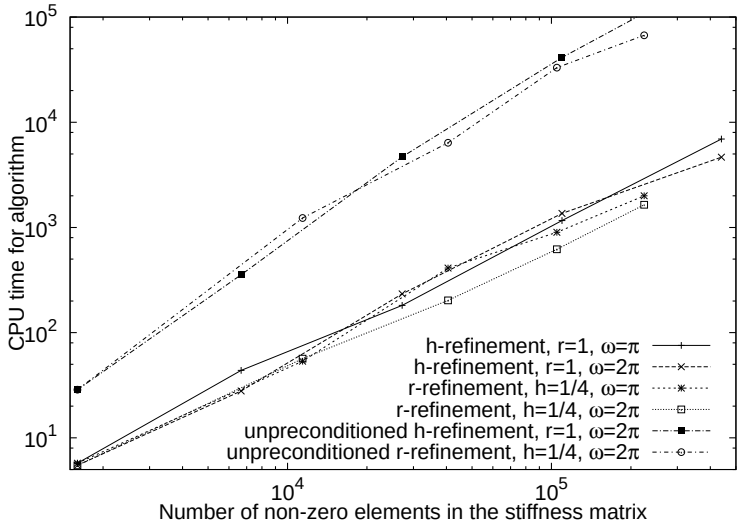

Figure 4. CPU time of h- and r-refinements in seconds.

pollution term is clearly visible in the error curves. We expected to see a more pronounced reduction in the pollution effect with higher orders. Now it is almost similar with all orders. Perhaps the difference could be observed by extending the test to higher wave numbers.

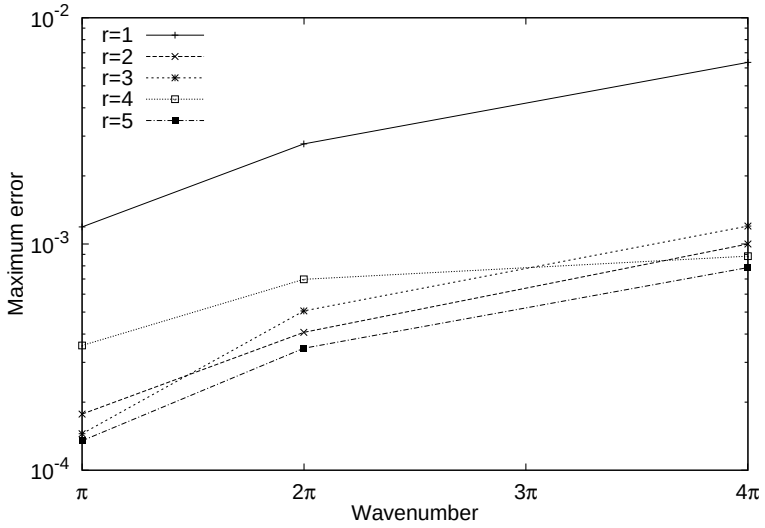

Figure 5. Behaviour of the error with respect to the wavenumber for different orders of the polynomial basis such that $\lambda/h = 2^{7-r}$.

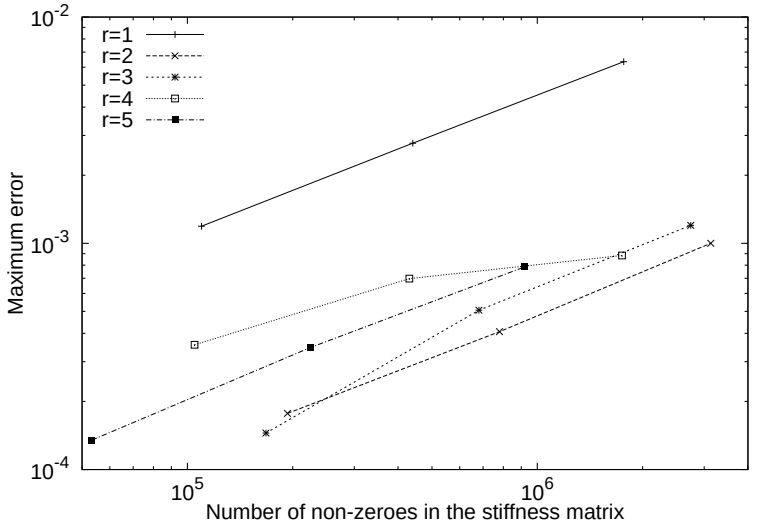

Figure 6. Behaviour of the error with respect to the non-zero elements in the stiffness matrix such that $\lambda/h = 2^{7-r}$.

Fig. 6 shows the same errors in terms of the number of nonzero matrix entries. These results support the conclusion that certain error level is reached more efficiently by applying higher order spatial discretization.

Type of the obstacle		r 1	2	3	4	5
non-convex semi-open cavity	DOF	2112	8064	17856	31488	48960
	iter	152	123	122	122	122
two non-convex semi-open cavities	DOF	1221	4635	10241	18039	28029
	iter	90	95	95	95	95
convex cavity (square)	DOF	864	3264	7200	12672	19680
	iter	45	65	45	45	41

Table 1
Number of iterations (iter) and degrees of freedom (DOF) with different scatterers.

5.2 Scattering examples

In this section, we consider ordinary scattering problems (8)-(11), where $f = 0$, $y_{\text{ext}} = \frac{\partial u_{\text{inc}}}{\partial \mathbf{n}} + \frac{\partial u_{\text{inc}}}{\partial t}$, and the incident plane wave is of the form $u_{\text{inc}}(\mathbf{x}, t) = \cos(\omega t - \vec{\omega} \cdot \mathbf{x})$. We use the propagation direction $\vec{\omega} = \omega\Big(-\frac{\sqrt{3}}{2}, \frac{1}{2}\Big)$, angular frequency $\omega = 3\pi$, and mesh stepsize $h = \frac{1}{8}$. There are slightly over five elements per wavelength. To guarantee demands for accuracy also for higher orders, we have chosen to use 600 timesteps per one time period $[0, T]$, and the stopping criterion works with $norm = \sqrt{c}$ and $\varepsilon = 10^{-3}$.

In the first scattering problem, the lower left corner of the domain surrounding the obstacle is at the point $(0.0, 0.0)$ and the upper right corner is at the point $(7.75, 4.25)$. Internal width and height of the cavity are 5 and $\frac{5}{4}$, and thickness of the wall is $\frac{1}{4}$ (see Fig. 7). The second scattering problem is solved in rectangle $[0, 5] \times [0, 4]$, where we have two non-convex semi-open cavities (see Fig. 8). Internal width and height of each cavity is $\frac{3}{4}$ and $\frac{5}{4}$. Thickness of the wall is $\frac{1}{4}$, and distance between cavities is 1. We also consider scattering by the same square obstacle as in the previous section. Number of iterations with different scatterers are shown in Tbl. 1, and contour plots of the numerical solutions with $r = 3$ are in Figs. 7-9.

As we can see, the number of iterations is substantially less in the case of convex square scatterer than in the cases of non-convex scatterers. In all the experiments it appears that preconditioning keeps the number of CG iterations bounded with respect to r.

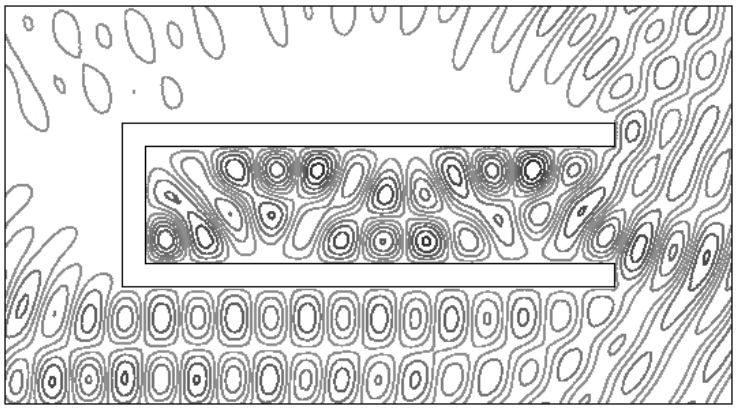

Figure 7. Contourplot of scattering by a non-convex semi-open cavity.

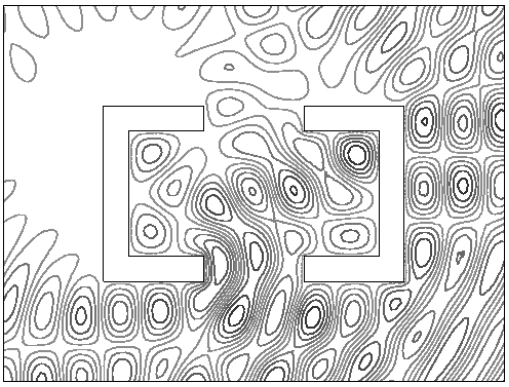

Figure 8. Contourplot of scattering by two non-convex semi-open cavities.

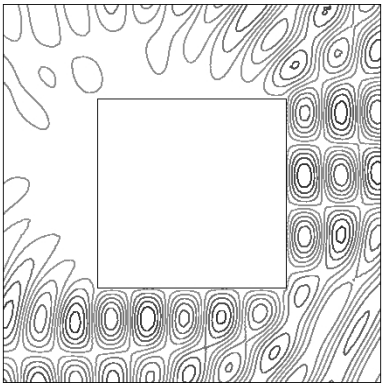

Figure 9. Contourplot of scattering by a square.

6 Conclusions

The spectral element discretization used in this article results in a global mass matrix that is diagonal by construction. No inversion of a mass matrix is needed, which leads to a very efficient implementation of the control algorithm. With the higher-order spectral element method, certain error level can be reached with lower computational work than with conventional FEM.

Computational effort of the method seems to have linear dependence on the number of non-zero elements in the stiffness matrix. The number of preconditioned CG iterations appears to be independent of the order of the spectral element basis, which confirms the efficiency of the AMG preconditioner, and makes the solver feasible for higher orders.

It is worth mentioning that the time discretization used here is only second order accurate, which restrict the efficiency of the scheme with higher order elements. In future, it could be of interest to use more accurate, i.e. higher order, time schemes.

Acknowledgements

This work was funded by Finnish Foundation for Technology (TES) and National Technology Agency of Finland (TEKES). The authors are grateful to Dr. Jari Toivanen and Dr. Janne Martikainen for useful discussions.

References

[1] B. Engquist, A. Majda, Radiation boundary conditions for acoustic and elastic wave calculations, Communications on Pure and Applied Mathematics 32 (1979) 313–357.

[2] Y. A. Erlangga, C. Vuik, C. W. Oosterlee, On a class of preconditioners for solving the Helmholtz equation, Applied Numerical Mathematics 50 (3-4) (2004) 409–425.

[3] Y. A. Erlangga, C. W. Oosterlee, C. Vuik, A novel multigrid based preconditioner for heterogeneous Helmholtz problems, SIAM Journal on Scientific Computing 27 (4) (2006) 147–149.

[4] F. Ihlenburg, Finite Element Analysis of Acoustic Scattering, Springer Verlag, 1998.

[5] C. Farhat, P. Wiedemann-Goiran, R. Tezaur, A discontinuous Galerkin method with plane waves and Lagrange multipliers for the solution of short wave exterior Helmholtz problems on unstructured meshes, Wave Motion 39 (4) (2004) 307–317.

[6] T. Huttunen, J. P. Kaipio, P. Monk, The perfectly matched layer for the ultra weak variational formulation of the 3D Helmholtz equation, International Journal for Numerical Methods in Engineering 61 (7) (2004) 1072–1092.

[7] M. O. Bristeau, R. Glowinski, J. Périaux, Controllability methods for the computation of time-periodic solutions; application to scattering, Journal of Computational Physics 147 (2) (1998) 265–292.

[8] J. L. Lions, Exact controllability, stabilization and perturbations for distributed systems, SIAM Review 30 (1) (1988) 1–68.

[9] R. Glowinski, J. Périaux, J. Toivanen, Time-periodic solutions of wave equation via controllability and fictitious domain methods, in: G. Cohen, E. Heikkola, P. Joly, P. Neittaanmäki (Eds.), Mathematical and Numerical Aspects of Wave Propagation, Proceedings of WAVES 2003, Springer, Jyväskylä, Finland, 2003, pp. 805–810.

[10] G. Cohen, Higher-Order Numerical Methods for Transient Wave Equations, Springer Verlag, 2001.

[11] O. Z. Mehdizadeh, M. Paraschivoiu, Investigation of a two-dimensional spectral element method for Helmholtz's equation, Journal of Computational Physics 189 (2003) 111–129.

[12] E. Heikkola, S. Mönkölä, A. Pennanen, T. Rossi, Solving the acoustic scattering problem with controllability and spectral element methods, Reports of the Department of Mathematical Information Technology, Series B. Scientific Computing, B 3/2006, Department of Mathematical Information Technology, University of Jyväskylä (2006).

[13] F. Kickinger, Algebraic multi-grid for discrete elliptic second-order problems, in: Multigrid methods V (Stuttgart, 1996), Springer, Berlin, 1998, pp. 157–172.

[14] J. Martikainen, A. Pennanen, Application of an algebraic multigrid method to incompressible flow problems, Reports of the Department of Mathematical Information Technology, Series B. Scientific Computing, B 2/2006, Department of Mathematical Information Technology, University of Jyväskylä, submitted to Journal of Computational Physics (2006).

[15] J. Heys, T. Manteuffel, S. McCormick, L. Olson, Algebraic multigrid for higher-order finite elements, Journal of Computational Physics 204 (2) (2005) 520–532.